

On stability prediction for milling

Janez Gradišek^{a,*}, Martin Kalveram^b, Tamás Insperger^c, Klaus Weinert^b,
Gábor Stépán^c, Edvard Govekar^a, Igor Grabec^a

^aFaculty of Mechanical Engineering, University of Ljubljana, Aškerčeva 6, SI-1000 Ljubljana, Slovenia

^bDepartment of Machining Technology (ISF), University of Dortmund, Baroper Straße 301, D-44227 Dortmund, Germany

^cDepartment of Applied Mechanics, Budapest University of Technology and Economics, H-1521 Budapest, Hungary

Received 25 May 2004; accepted 16 November 2004

Available online 8 January 2005

Abstract

Stability of 2-dof milling is investigated. Stability boundaries are predicted by the zeroth order approximation (ZOA) and the semi-discretization (SD) methods. While similar for high radial immersions, predictions of the two methods grow considerably different as radial immersion is decreased. The most prominent difference is an additional type of instability causing periodic chatter which is predicted only by the SD method. Experiments confirm predictions of the SD method, revealing three principal types of tool motion: periodic chatter-free, quasi-periodic chatter and periodic chatter, as well as some special chatter cases. Tool deflections recorded during each of these motion types are studied in detail.

© 2004 Elsevier Ltd. All rights reserved.

Keywords: End milling; Stability prediction

1. Introduction

High material removal rates, provided in theory by the modern machining centers, often cannot be achieved in practice due to the inherent instability of a cutting process. In cutting processes which involve rotation of the tool or workpiece, the instability is caused by the so called regeneration of surface waviness during successive cuts: wavy surface left behind by the previous cut influences chip thickness during the current cut, thereby contributing to the wavy surface, which in turn influences chip thickness in the successive cut, etc. The resulting instability is called regenerative chatter.

Dynamics of regenerative cutting processes can be described by models in the form of linear delay-differential equations (DDEs) [1,2]. Chatter-free cutting and chatter correspond respectively to the linearly stable and unstable solutions of the model equations. The cutting parameters that assure stable, chatter-free machining can therefore be

predicted by the linear stability analysis of the equations. The stability boundary is usually presented in a graph of the maximal chatter-free depth of cut vs. spindle speed. The graph is called a stability chart.

For continuous cutting, such as uninterrupted turning, the model equations are autonomous and the stability boundary can be given in closed form. The stability boundary has a typical ‘lobed’ structure, with stability maxima located at spindle speeds corresponding to the integer fractions of the eigen-frequencies of the most flexible modes of the machine–tool–workpiece system. The instability, i.e. the transition from chatter-free cutting to chatter, corresponds to the sub-critical Hopf bifurcation [3,4].

For interrupted machining, such as milling and interrupted turning, the cutting force variation is time-periodic. The resulting model equations are non-autonomous DDEs for which the linear stability condition cannot be given in closed form. The stability boundary can be determined numerically, by time domain simulations [5–7]. While indispensable for the study of complicated cutting process models which involve trochoidal tool path, multiple regeneration effects, non-linear force dependencies, etc., the time domain simulations are an inefficient way of

* Corresponding author. Tel.: +386 1 4771 166; fax: +386 1 2518 567.
E-mail address: janez.gradisek@fs.uni-lj.si (J. Gradišek).

exploring the parameter space of linear DDEs. The first analytical attempts at stability prediction of milling were based on Fourier expansion of the time-periodic force coefficient [8,9]. The accuracy of the obtained stability boundary depends on the shape of the cutting force variation and the number of Fourier terms used to approximate it. For cutters with a large number of teeth and for substantial radial immersions, the cutting force varies relatively little so that reasonably accurate stability predictions can be achieved by using only the zeroth order Fourier term [10,11]. However, for cutters with few teeth and for low radial immersions, prohibitively many Fourier terms may be needed to capture the cutting force variation. In such cases, which are quite common in high-speed milling, the exact stability boundary may differ significantly from the one predicted by the zeroth order approximation (ZOA).

This discrepancy was first shown for the case of very low immersion milling, where the time interval of tool–workpiece contact was a small fraction of the spindle period [12,13]. Based on a discrete representation of the impact-like cutting process combined with the exact analytical solution of the free tool vibration, a time-domain analytical method for stability prediction was developed which revealed that there exist two types of instability in milling: the Hopf bifurcation, which causes the quasi-periodic chatter, and the period doubling or flip bifurcation, which causes the periodic chatter. The stability boundary in milling therefore consists of two sets of lobes corresponding to the two instability types. In contrast, the ZOA method predicts only one type of instability, the Hopf bifurcation.

The stability predictions from Refs. [12,13] lose accuracy as the time of the tool–workpiece contact increases. Two alternative methods have since been proposed that can predict stability boundary for an arbitrary time in the cut. The first method combines the exact analytical solution of the free tool vibration with the approximate solution for the tool vibration during cutting calculated using temporal finite element analysis (TFEA) [14]. The second method employs the semi-discretization (SD) scheme to transform the DDE into a series of autonomous ordinary differential equations (ODEs) for which the solutions are known [15]. In both methods, stability is determined by the eigen-values of the transition matrix which connects the solutions between successive cuts. The methods have been derived and verified experimentally using a 1-dof milling system [16,17]. Recently, both methods have also been extended to 2-dof milling systems [18–20].

In this paper, stability of a 2-dof milling system is investigated. Stability boundaries are predicted using the ZOA and SD methods. The ZOA method is briefly reviewed and the SD method for 2-dof systems is presented. Stability predictions of the two methods are compared for a series of radial immersions and verified experimentally on a high-speed milling center using a long and slender tool. The recorded tool deflections in the X – Y plane are analyzed in

detail and six different types of tool motion are distinguished: three principal types predicted by the SD method (periodic chatter-free, quasi-periodic and periodic chatter) as well as three special chatter cases.

2. Stability prediction for end milling

Consider a 2-dof end milling operation shown schematically in Fig. 1. A cutter with a diameter D and N equally spaced teeth rotates at a constant angular velocity Ω . The radial immersion angle of the j -th tooth varies with time as: $\phi_j(t) = \Omega t + 2\pi(j-1)/N$. A compliant machine–tool structure is excited by the tangential (F_t) and radial (F_r) components of the milling force at the tool tip causing dynamic response of the structure governed by the following equation:

$$M\ddot{X}(t) + C\dot{X}(t) + KX(t) = F(t). \quad (1)$$

Here, $X(t)$ and $F(t)$ denote the displacement and cutting force vectors, while M , C and K denote the system mass, damping and stiffness matrices. For a system with m vibration modes in X and Y directions, the vectors are $2m \times 1$ and the matrices $2m \times 2m$ dimensional. The matrices are diagonal if the modes in X and Y directions are uncoupled.

The feed (F_x) and normal (F_y) cutting force components acting on the j -th tooth are given by:

$$\begin{aligned} F_{x,j}(t) &= [-F_{t,j}(t) \cos \phi_j(t) - F_{r,j}(t) \sin \phi_j(t)]g_j(t), \\ F_{y,j}(t) &= [F_{t,j}(t) \sin \phi_j(t) - F_{r,j}(t) \cos \phi_j(t)]g_j(t), \end{aligned} \quad (2)$$

where $g_j(t)$ represents a unit step function determining whether or not the j -th tooth is cutting. The tangential and radial cutting force components are assumed proportional to the chip load defined by the chip thickness $h_j(t)$ and axial

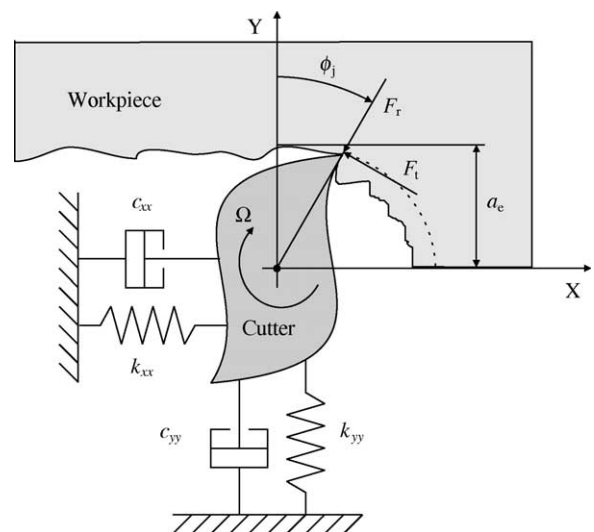


Fig. 1. Schematic diagram of end milling.

depth of cut a_p (or chip width):

$$F_{t,j}(t) = K_t a_p h_j(t), \quad F_{r,j}(t) = K_r a_p h_j(t) = k_r F_{t,j}(t). \quad (3)$$

K_t and K_r denote the specific cutting force coefficients, while k_r denotes their ratio, $k_r = K_r/K_t$.

The instantaneous chip thickness consists of a static component due to the feed motion, $h_{s,j}(t) = f_z \sin \phi_j(t)$ with feed per tooth f_z , and the dynamic component $h_{d,j}(t)$ due to the cutter displacement. Stability of cutting is influenced only by the latter which is given by:

$$h_{d,j}(t) = [\Delta x(t, T) \sin \phi_j(t) + \Delta y(t, T) \cos \phi_j(t)] g_j(t), \quad (4)$$

where $\Delta x(t, T) = x(t) - x(t - T)$ and $\Delta y(t, T) = y(t) - y(t - T)$ describe the surface regeneration, i.e. the difference between the tool positions at the present and previous tooth passes. $T = 2\pi/N\Omega$ is the tooth passing period.

The total cutting force acting on the cutter is obtained by summing the contributions of all cutting edges:

$$\begin{bmatrix} F_x(t) \\ F_y(t) \end{bmatrix} = a_p K_t \begin{bmatrix} A_{xx}(t) & A_{xy}(t) \\ A_{yx}(t) & A_{yy}(t) \end{bmatrix} \begin{bmatrix} \Delta x(t, T) \\ \Delta y(t, T) \end{bmatrix}. \quad (5)$$

Here, $A_{ij}(t)$ denote the directional dynamic milling force coefficients which vary periodically in time with the tooth passing period T , $A_{ij}(t) = A_{ij}(t + T)$:

$$\begin{aligned} A_{xx}(t) &= \frac{1}{2} \sum_{j=1}^N [-\sin 2\phi_j(t) - 2k_r \sin^2 \phi_j(t)] g_j(t), \\ A_{xy}(t) &= \frac{1}{2} \sum_{j=1}^N [-2 \cos^2 \phi_j(t) - k_r \sin 2\phi_j(t)] g_j(t), \\ A_{yx}(t) &= \frac{1}{2} \sum_{j=1}^N [2 \sin^2 \phi_j(t) - k_r \sin 2\phi_j(t)] g_j(t), \\ A_{yy}(t) &= \frac{1}{2} \sum_{j=1}^N [\sin 2\phi_j(t) - 2k_r \cos^2 \phi_j(t)] g_j(t). \end{aligned} \quad (6)$$

Finally, the governing delay differential equation (DDE) of motion reads:

$$M\ddot{\mathbf{X}}(t) + C\dot{\mathbf{X}}(t) + \mathbf{K}\mathbf{X}(t) = a_p K_t \mathbf{A}(t)(\mathbf{X}(t) - \mathbf{X}(t - T)). \quad (7)$$

Time dependence of the directional force coefficients $\mathbf{A}(t)$ complicates the stability analysis of Eq. (7) so that the stability boundary generally cannot be determined in closed form. A possible solution to this problem is to expand the coefficients in a Fourier series and retain the terms needed for the approximation [8,9,11]. In the simplest case, which is briefly reviewed below, only the zeroth order Fourier term is kept. Such an approximation is practical as it allows a closed form expression of the stability boundary, but it loses accuracy as the radial immersion and the number of cutter teeth decrease. Alternatively, stability analysis can be carried out in the time domain using the recently proposed

methods [13–15]. One of them, the semi-discretization method (SD) [15], is presented in Section 2.2.

2.1. Zeroth order approximation method

The zeroth order approximation method was proposed in Ref. [11]. It is based on approximating the periodic directional milling force coefficient (Eq. (6)) by its average value, $\mathbf{A}(t) \approx \mathbf{A}_0$. The resulting approximate milling force vector is:

$$\mathbf{F}(t) = a_p K_t \mathbf{A}_0 (\mathbf{X}(t) - \mathbf{X}(t - T)). \quad (8)$$

The cutter displacement caused by the milling force \mathbf{F} can be expressed in the Laplace domain by means of a frequency response function (FRF) matrix \mathbf{H} of the machine–tool structure as:

$$\begin{bmatrix} x(s) \\ y(s) \end{bmatrix} = \begin{bmatrix} H_{xx}(s) & H_{xy}(s) \\ H_{yx}(s) & H_{yy}(s) \end{bmatrix} \begin{bmatrix} F_x(s) \\ F_y(s) \end{bmatrix}. \quad (9)$$

Combining Eqs. (8) and (9) gives a system of equations:

$$[\mathbf{I} + \Lambda(s)\mathbf{A}_0\mathbf{H}(s)]\mathbf{F}(s) = 0, \quad (10)$$

where $\Lambda(s) = -a_p K_t (1 - e^{-sT})$ is introduced and \mathbf{I} denotes 2×2 identity matrix. The system in Eq. (10) has a non-trivial solution only if its determinant is zero:

$$\det[\mathbf{I} + \Lambda(s)\mathbf{A}_0\mathbf{H}(s)] = 0. \quad (11)$$

Signs of the real parts of the roots s of Eq. (11) determine the linear stability of the system. On the stability boundary, the real part is zero, so that $s = i\omega_c$, where ω_c denotes the chatter frequency. Substituting $s = i\omega_c$ into Eq. (11), a quadratic equation for Λ is obtained, solving which yields the expressions for the depth of cut a_p at the stability boundary and for the corresponding spindle speed n , given the chatter frequency ω_c . Further details on this procedure can be found in Refs. [9,11].

Two remarks about this method should be pointed out here. First, as noted in Ref. [11], calculation of the stability boundary is simplified if the FRF matrix \mathbf{H} is assumed diagonal, i.e. the vibration modes in X and Y directions are assumed uncoupled and the cross FRFs are set to zero, $H_{xy}(s) = H_{yx}(s) = 0$. If this assumption holds, it simplifies not only the calculations but also the measurements of the machine–tool FRF and identification of the modal properties. On the other hand, if mode coupling is indeed present it should not be neglected. A numerical experiment reveals that even weak mode coupling, with cross terms in magnitude only 2% that of the direct terms, may already influence the predicted stability boundary in case of low radial immersion (compare solid vs. dashed lines in Fig. 2). Numerical investigations also show that the effect of mode coupling on stability boundary becomes more pronounced as radial immersion is decreased. This indicates that it may be reasonable to check for the presence of vibration mode

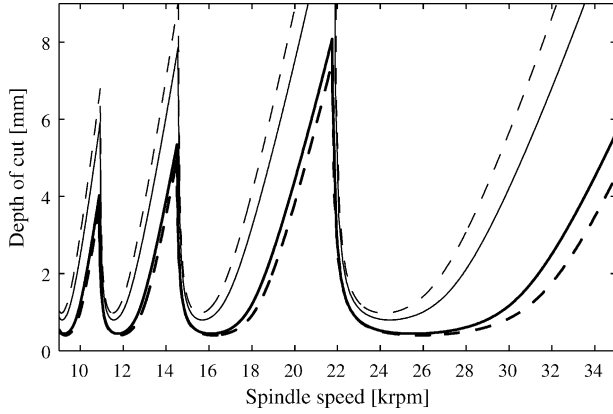


Fig. 2. Stability boundaries for the diagonal (solid lines) and full transfer matrices (dashed lines). Thick and thin lines correspond to the two solutions for A . Cutting parameters: up-milling, $a_e=0.1D$, $K_t=644$ MPa, $k_r=0.37$. Modal parameters in Table 1 and $m_{xy}=m_{yx}=0.04$ g, $c_{xy}=c_{yx}=0.032$ kg/s and $k_{xy}=k_{yx}=8.2$ kN/m.

coupling, particularly if stability boundary is to be predicted for low radial immersion milling.

Second, there exist two solutions of the quadratic equation for A , namely a complex conjugated pair A_1 and $A_2 = A_1^*$, which yield two different stability boundaries. The procedure itself does not indicate which solution is the correct one. According to the experience of the authors, one of the boundaries has usually, but not always (compare for example thick vs. thin lines in Fig. 2), unrealistically high values of the depth of cut even at the stability minima, which clearly distinguishes it from the correct boundary. It seems therefore advisable to calculate both stability boundaries and to choose the one with the lowest values of a_p .

2.2. Semi-discretization method

Semi-discretization is a technique often used in computational fluid mechanics for solving partial differential equations (PDEs). The idea is to discretize the PDE along the spatial coordinates while leaving the time coordinate unchanged. In Ref. [15], the method was adapted to the analysis of delay differential equations (DDEs) where the time delayed terms are approximated by a piecewise constant function while the current time terms are left unchanged. The DDE is thereby approximated by a series of ordinary differential equations (ODEs). The semi-discretization method has already been verified and successfully applied to the stability analysis of various DDEs, including those of 1-dof and 2-dof milling systems [16,17,20]. Here, the method is presented for the 2-dof case [20].

The governing DDE for a 2-dof milling system is given by Eq. (7). Letting $Q(t) = -a_p K_t A(t)$ to simplify the notation, the DDE may be rearranged as:

$$M\ddot{X}(t) + C\dot{X}(t) + (K + Q(t))X(t) = Q(t)X(t-T). \quad (12)$$

The discretization is introduced using a time interval $\Delta t = [t_i, t_{i+1}]$. The delay time becomes $T = m\Delta t$, where m is an integer determining coarseness of the discretization. The periodic cutting force coefficient $Q(t)$ and the delayed state $X(t-T)$ are approximated by:

$$Q(t) \approx Q(t_i) = Q_i,$$

$$X(t-T) \approx \frac{1}{2}(X(t_{i-m+1}) + X(t_{i-m})) = \frac{1}{2}(X_{i-m+1} + X_{i-m}). \quad (13)$$

The DDE in Eq. (12) is herewith transformed into a series of autonomous (ODEs) with piecewise constant excitation on the right hand side:

$$M\ddot{X}(t) + C\dot{X}(t) + (K + Q_i)X(t) = \frac{Q_i}{2}(X_{i-m+1} + X_{i-m}). \quad (14)$$

The second order ODEs can be written as systems of first order ODEs:

$$\dot{u}(t) = W_i u(t) + V_i(u_{i-m+1} + u_{i-m}) = W_i u(t) + w_i, \quad (15)$$

where $u = [\dot{x}, \dot{y}, x, y]^T$. For the initial condition $u(t_i) = u_i$, the solution of Eq. (15) is known:

$$u(t) = e^{W_i(t-t_i)}(u_i + W_i^{-1}w_i) - W_i^{-1}w_i. \quad (16)$$

Substituting $t = t_{i+1}$ and $u(t_{i+1}) = u_{i+1}$ into the solution gives:

$$\begin{aligned} u_{i+1} &= e^{W_i \Delta t} u_i + (e^{W_i \Delta t} - I)W_i^{-1}V_i(u_{i-m+1} + u_{i-m}) \\ &= P_i u_i + R_i(u_{i-m+1} + u_{i-m}). \end{aligned} \quad (17)$$

Eq. (17) can be recast into a discrete map of the form:

$$v_{i+1} = Z_i v_i, \quad (18)$$

with the state vector $v_i = [u_i, u_{i-1}, \dots, u_{i-m}]^T$ and the coefficient matrix:

$$Z_i = \begin{bmatrix} P_i & 0 & 0 & \dots & 0 & R_i & R_i \\ I & 0 & 0 & \dots & 0 & 0 & 0 \\ 0 & I & 0 & \dots & 0 & 0 & 0 \\ \vdots & \vdots & \vdots & \ddots & \vdots & \vdots & \vdots \\ 0 & 0 & 0 & \dots & I & 0 & 0 \\ 0 & 0 & 0 & \dots & 0 & I & 0 \end{bmatrix}. \quad (19)$$

The Floquet transition matrix over the principal period T is approximated by coupling the solutions of m successive time intervals Δt :

$$\Phi = Z_{m-1}Z_{m-2}\dots Z_1Z_0. \quad (20)$$

Stability of the investigated system is determined by the eigen-values of the transition matrix Φ . The system is stable if all eigen-values of Φ are in modulus less than 1.

In the case of milling, two types of instability are possible:

- (1) The eigen-value is complex and its modulus becomes larger than 1. This case corresponds to the Hopf bifurcation, which causes chatter characterized by quasi-periodic vibrations.
- (2) The eigen-value is real and its value becomes smaller than -1 . This case corresponds to the period doubling or flip bifurcation, which causes chatter characterized by periodic vibrations.

The routes to instability for Hopf and flip bifurcations are illustrated by the eigen-value trajectories in the bottom panels of Fig. 3, together with a segment of a stability chart and the depth of cut and spindle speed values corresponding to the trajectory points (top panel). In the case of a Hopf bifurcation (bottom left panel), a pair of complex conjugated eigen-values penetrates the unit circle in the complex plane, whereas in the case of a flip bifurcation (bottom right panel), the unit circle is penetrated by one real and negative eigen-value.

Finally, note that the computational burden of the SD method can be greatly reduced if the unnecessary components of the discrete state vector v_i , are left out. For the 2-dof case with a single mode in both X and Y directions, the state vector must have at least the following $2(m+2)$ components:

$$\tilde{v}_i = [\dot{x}_i, \dot{y}_i, x_i, y_i, x_{i-1}, y_{i-1}, \dots, x_{i-m+1}, y_{i-m+1}, x_{i-m}, y_{i-m}]^T. \quad (21)$$

The corresponding coefficient matrix is:

$$\tilde{Z}_i = \begin{bmatrix} P_{i,11} & P_{i,12} & P_{i,13} & P_{i,14} & 0 & \dots & 0 & R_{i,13} & R_{i,14} & R_{i,13} & R_{i,14} \\ P_{i,21} & P_{i,22} & P_{i,23} & P_{i,24} & 0 & \dots & 0 & R_{i,23} & R_{i,24} & R_{i,23} & R_{i,24} \\ P_{i,31} & P_{i,32} & P_{i,33} & P_{i,34} & 0 & \dots & 0 & R_{i,33} & R_{i,34} & R_{i,33} & R_{i,34} \\ P_{i,41} & P_{i,42} & P_{i,43} & P_{i,44} & 0 & \dots & 0 & R_{i,43} & R_{i,44} & R_{i,43} & R_{i,44} \\ 0 & 0 & 1 & 0 & 0 & \dots & 0 & 0 & 0 & 0 & 0 \\ 0 & 0 & 0 & 1 & 0 & \dots & 0 & 0 & 0 & 0 & 0 \\ 0 & 0 & 0 & 0 & 1 & \dots & 0 & 0 & 0 & 0 & 0 \\ \vdots & \ddots & \vdots & \vdots & \vdots \\ 0 & 0 & 0 & 0 & 0 & \dots & 1 & 0 & 0 & 0 & 0 \\ 0 & 0 & 0 & 0 & 0 & \dots & 0 & 1 & 0 & 0 & 0 \\ 0 & 0 & 0 & 0 & 0 & \dots & 0 & 0 & 1 & 0 & 0 \end{bmatrix}, \quad (22)$$

where $P_{i,hj}$ and $R_{i,hj}$ are the elements of matrices P_i and R_i in the h -th row and j -th column, respectively. Further details on semi-discretization method for stability analysis can be found in Refs. [15,20,21].

3. Experimental results

The cutting tests were conducted on a high speed milling center using a cylindrical end mill with a single cutting edge ($N=1$), $D=8$ mm diameter, 45° helix angle, and $L=96$ mm overhang ($L/D=12$). Originally, the cutter had two teeth but one tooth was removed in order to avoid disturbances due to the tool runout. A large overhang resulting in a very long and slender tool was used to assure a single dominant vibration mode of the tool. The purpose of these two simplifications was to provide clearer demonstration and facilitate better understanding of the dynamic properties of the milling process. The simplifications were not imposed by the described semi-discretization method, which is generally applicable and not restricted to cases with a single vibration mode.

The cutter was mounted in a HSK40E shrink fit holder. The workpiece was a square block made of AlMgSi0.5 aluminum alloy, for which the specific tangential force coefficient and the force ratio were determined mechanically [22,23]: $K_t=644$ MPa and $k_r=0.37$. Minimal amount of coolant was used.

Tool deflections during cutting were measured in X and Y directions simultaneously by a couple of laser optical displacement sensors mounted on the spindle housing. The sampling rate of the sensors was 10 kHz. The spindle housing was considered rigid since its vibration during cutting was found to be negligible compared to the deflections of the highly flexible tool. The measurement point on the tool shaft was located 65 mm above the tool tip. The recorded tool deflections were mainly associated with the first bending mode of the tool. Deflections at the tool tip

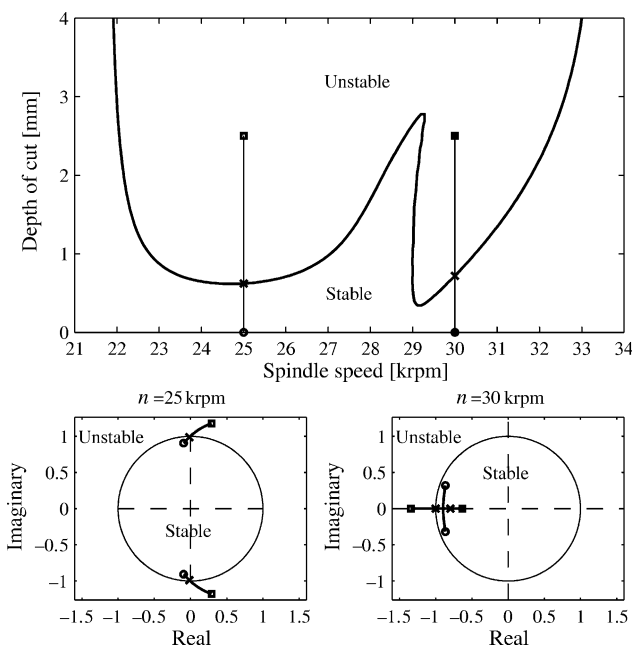


Fig. 3. Segment of a stability chart (top). Eigen-value trajectories for Hopf (left) and flip bifurcations (right) (bottom). The points below (circles), on (crosses), and above (squares) the stability boundary correspond respectively to all eigen-values inside, at least one eigen-value on, and at least one eigen-value outside the unit circle in the complex plane. Cutting parameters: up-milling, $a_c=0.05D$, $K_t=644$ MPa, $k_r=0.37$. Modal parameters in Table 1.

could therefore be calculated by an appropriate scaling of the recorded deflections.

A photo diode was attached to the spindle housing in order to detect a black/white transition painted on the rotating tool holder. The transition occurred once per tool revolution giving a signal synchronized with the spindle rotation. The signal was used in off-line stroboscope resampling of the deflection records.

3.1. Identification of modal parameters

The frequency response function (FRF) matrix $\mathbf{H}(s)$ of the machine–tool structure was determined by a standard impact test procedure. For stability prediction, the FRF at the tool tip is required, i.e. both the excitation and the response should be located at the tool tip (tip–tip FRF). However, due to the flexible tool of a relatively small diameter, the excitation at the tool tip using a standard instrumented hammer with a 100 g head was not impulse-like. Regular excitation could only be assured by hitting the tool at the shaft below the tool holder. Consequently, the FRF at the tool tip could not be measured directly, instead it had to be calculated from the FRFs with excitation at the tool shaft. To facilitate such a calculation, the tool response was measured simultaneously at the excitation point (15 mm below the tool holder) and at the tool tip, yielding shaft–shaft and shaft–tip FRFs. In order to check for the presence of mode coupling, the tool response was measured in X and Y directions at both locations. For this purpose, two pairs of low mass accelerometers (0.7 g each) were attached to the tool at the two locations. The measured FRFs were curve fit using a commercial modal analysis software to identify the modal parameters and obtain the modal matrix, which was then used to calculate the tip–tip FRF.

The measured shaft–tip and predicted tip–tip FRFs are compared in Fig. 4. Due to the large overhang of the tool, the FRFs are dominated by a single peak at $f_t \approx 722$ Hz. It

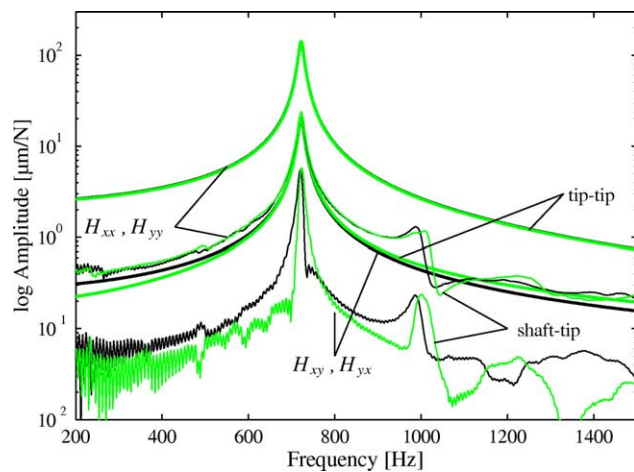


Fig. 4. Measured shaft–tip (thin) and predicted tip–tip (thick) FRFs: H_{xx} (top black), H_{yy} (bottom black), H_{yx} (bottom grey), and H_{xy} (top grey).

Table 1
System matrices for the tip–tip FRF

	xx	yy
Mass \mathbf{M} (g)	20.1	19.9
Damping \mathbf{C} (kg/s)	1.56	1.60
Stiffness \mathbf{K} (kN/m)	414	409

xx and yy denote the indices of the diagonal matrix elements.

was confirmed by finite element modeling that this frequency corresponds approximately to the first bending mode of the tool. A small peak observed at $f \approx 1000$ Hz corresponds to the spindle vibration mode. This mode was found to have no influence on the cutting stability and was therefore neglected in the modal identification procedure. The frequencies and amplitudes of the dominant modes in X and Y directions are almost the same so that the direct FRFs (H_{xx} and H_{yy}) are practically overlapping. As expected, the amplitude of the tip–tip FRFs is much higher than that of the shaft–tip FRFs. The amplitude of cross FRFs (H_{xy} and H_{yx}) is almost an order of magnitude smaller than that of the direct FRFs, which indicates that mode coupling is indeed very weak.

The diagonal elements of the system matrices \mathbf{M} , \mathbf{C} , and \mathbf{K} for the tip–tip FRFs are listed in Table 1. The out-of-diagonal elements of these matrices were much smaller and their calculation was quite unreliable. Consequently, the out-of-diagonal elements of the system matrices were set to zero which means that mode coupling was neglected.

3.2. Predicted stability charts

Stability charts were predicted by the zeroth order approximation (ZOA) and the semi-discretization (SD) methods for a series of radial depths of cut a_e .

Charts for up-milling with $a_e = D, 0.5D, 0.10D$ and $0.05D$ are compared in Fig. 5. For $a_e = D$ and $0.5D$, ZOA and SD methods yield similar results: lobed stability boundaries, with stability maxima located at the integer fractions of the dominant eigen-frequency, $n = (f_t/kN)60$ rpm. Note that only the lobes for $k=2,3$, and 4 are shown in Fig. 5, and $N=1$ in the present study. These stability boundaries correspond to the instability called Hopf bifurcation which causes quasi-periodic chatter. As the radial depth of cut a_e is decreased, the discrepancy between the ZOA and SD stability boundaries grows considerably. The most prominent difference is an additional set of lobes introducing additional stable and unstable regions. The maxima of the new stable regions are located approximately at the odd integer fractions of twice the dominant eigen-frequency $n = (2f_t/(2k+1)N)60$ rpm. These lobes are predicted only by the SD method and, as shown below, correspond mainly to the instability called flip bifurcation which causes periodic chatter. They appear already at $a_e = 0.5D$ and grow steadily with decreasing a_e .

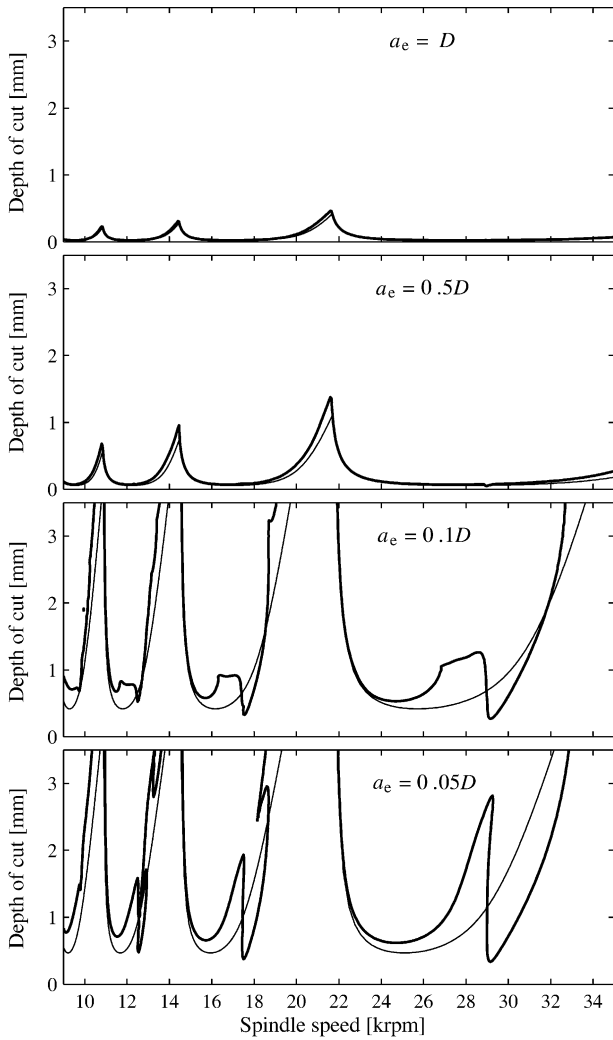


Fig. 5. Stability boundaries for up-milling at various radial immersions predicted by the ZOA (thin) and SD methods (thick).

For $a_e=0.05D$, the SD stability boundary has an intriguing structure; the lobe at $n \approx 12.5$ krpm is a closed curve within the stable domain, the lobe at $n \approx 18$ krpm is almost closed, and there are further lobe-like portions of the stability boundary at higher depths of cut. Such a stability boundary is similar to those predicted for a 1-dof interrupted turning system in Ref. [24], where it was proved rigorously that all flip bifurcation lobes for a 1-dof system, except for the first one at $n=2f_i \times 60$ rpm, are in fact closed curves distributed not only along the spindle speed axis, as the Hopf bifurcation lobes, but across the plane (n, a_p) . The present numerical investigations confirm that this property holds also for 2-dof milling systems. The flip bifurcation lobes shown superimposed on the stability chart for the $a_e = 0.05D$ case in top panel of Fig. 6 are indeed lens-like closed curves, distributed across the plane (n, a_p) . Similar results have been obtained also for other radial immersions.

The bifurcation scenario at the bottom and upper arcs of a lens-like flip lobe is illustrated in the bottom panels of Fig. 6

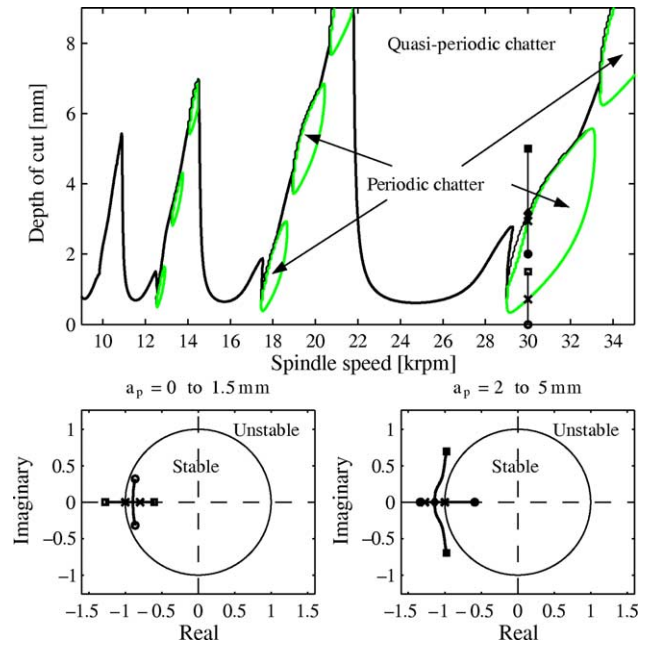


Fig. 6. Stability boundary for up-milling at $a_e=0.05D$ predicted by the SD method (top). Lines: thick black—overall stability boundary, thick grey—primary flip bifurcation boundary, thin black—boundary between the periodic and quasi-periodic chatter. Eigen-value trajectories for the primary flip bifurcation (left, denoted by crosses) and the secondary flip bifurcation (right, crosses) with the subsequent change of a pair of real eigen-values into a complex conjugate eigen-value pair (right, diamond) (bottom).

by trajectories of the two eigen-values of the Floquet transition matrix that determine stability and the type of vibrations arising when a_p is increased from 0 to 5 mm at $n = 30$ krpm, as indicated in the top panel stability chart. First, at $a_p \approx 0.77$ mm, one real eigen-value penetrates the unit circle in the complex plane, causing the primary flip bifurcation (bottom left panel) and the associated periodic chatter vibrations. This situation is identical to the one shown in the bottom right panel of Fig. 3. Next, at $a_p \approx 2.95$ mm, the second real eigen-value penetrates the unit circle (bottom right panel), causing the secondary flip bifurcation. The chatter vibrations remain periodic. At $a_p \approx 3.15$ mm, the two real eigen-values merge into a complex conjugated pair which changes the nature of chatter vibrations from periodic to quasi-periodic. The boundary between the periodic and quasi-periodic chatter vibrations is also shown superimposed on the stability chart in the top panel of Fig. 6. Except at $n = 29$ krpm, this boundary is almost indistinguishable from the upper arc of the flip bifurcation lobes.

Finally, comparing the size and location of Hopf and flip bifurcation lobes, it is important to note that although the Hopf lobes are much wider than the flip lobes, the latter usually reach to lower cutting depths than the former. Furthermore, the flip lobes may be located partly or even entirely within the stable domain corresponding to the Hopf lobes. In order to assure chatter-free machining, it is therefore necessary to consider both Hopf and flip bifurcation lobes when selecting the cutting parameters.

3.3. Experimental stability charts

The predicted stability boundaries were verified experimentally by cutting tests conducted at a series of spindle speeds n and depths of cut a_p . During each cut, a 100 mm long straight path was machined. A stable cut was performed before each recorded cut in order to assure the same reference surface for all cuts. Stability of cutting was assessed based on the recorded tool deflections, sound emitted during cutting, and roughness of the machined surface. The experimental and predicted stability charts for up-milling with $a_e = D$, $0.5D$, $0.10D$ and $0.05D$ are compared in Fig. 7. The results for down-milling are qualitatively similar (not shown).

For $a_e = D$ and $0.5D$, the predicted and experimental stability boundaries agree very well. In both cases, a flip bifurcation is found at $n = 29$ krpm, as predicted by the SD method. For $a_e = 0.5D$, a slight increase of the experimental

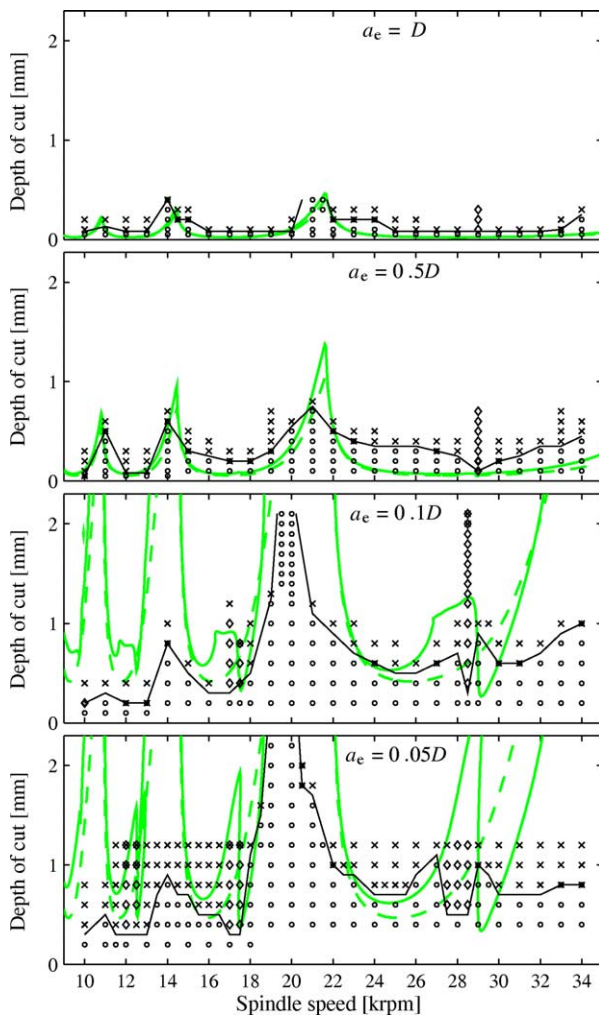


Fig. 7. Experimental and predicted stability boundaries for up-milling at various radial immersions. Circles—stable cutting, crosses—quasi-periodic chatter, diamonds—periodic chatter. Stability boundaries (lines): experimental (black), predicted by the SD (grey solid) and ZOA methods (grey dashed).

stability minima at higher spindle speeds is observed. Such a systematic increase of stability minima with spindle speed is observed also for lower radial immersions and for both milling directions. This phenomenon could be caused by a decrease of specific cutting force coefficients at higher spindle speeds.

For $a_e = 0.1D$ and $0.05D$, the predictions and experiments agree only qualitatively, i.e. with respect to the structure of the stability boundary. Several flip bifurcation lobes are found, all slightly below the predicted spindle speeds. Note that the flip lobes at $n = 17$ and 28.5 krpm for $a_e = 0.1D$ and at $n = 12$ and 17 krpm for $a_e = 0.05D$ appear to be bounded from above by the Hopf lobe. This indicates that the flip lobes might indeed be closed curves as predicted. The largest quantitative discrepancies between the predicted and experimental stability boundaries are observed at the stability maxima, which are significantly overestimated, while the stability minima are overestimated at low spindle speeds. It is presently not clear what causes these discrepancies. Possible reasons could be: (a) the variation of the radial immersion due to tool deflections and (b) the effect of the edge forces. The tool deflections during cutting affect the actual radial depth of cut a_e . Depending on the phase of vibrations, the tool deflections may either add or subtract from the nominal a_e , and thus either decrease or increase the actual stability boundary. The edge forces are caused by ploughing and rubbing of the tool [22] and are not accounted for in the simplified analytical model (Eq. (3)) used to predict the stability boundaries. According to the recent time domain simulations [7], the nonlinear effects of the edge forces may either decrease or increase the stability boundary.

Comparison of all four experimental stability charts in Fig. 7 also reveals that the locations of stability maximum at $n = (f_t/2)60 \approx 21$ krpm and the flip bifurcation lobe at $n = (2f_t/3)60 \approx 29$ krpm are shifted toward lower spindle speeds, $n \approx 20$ and 27.5 krpm, respectively, as radial immersion is decreased. Such a shift could be explained by variation of the dominant eigen-frequency of the tool with spindle speed, which becomes more pronounced at low radial immersions. In order to verify this assumption, the tool response to the impulse excitation was measured by the laser optical sensors at a series of spindle speeds. Due to the limitations of the experimental setup, these FRFs could not be used directly for stability prediction, but they do illustrate the influence of spindle speed on modal properties of the tool. The experiments show that the frequency and compliance of the dominant vibration mode both decrease as spindle speed is increased. Fig. 8 depicts the variation of the mode frequency f_t for the spindle speed range considered. At its minimum at $n = 23$ krpm, $f_t \approx 684$ Hz is approximately 5% lower than $f_t \approx 722$ Hz at zero spindle speed. If $f_t = 684$ Hz is used to calculate the location of the second flip bifurcation lobe, $n = (2f_t/3)60 \approx 27.4$ krpm is obtained, which agrees very well with the location of the flip lobe in the experimental stability chart for $a_e = 0.05D$ (bottom panel in Fig. 7).

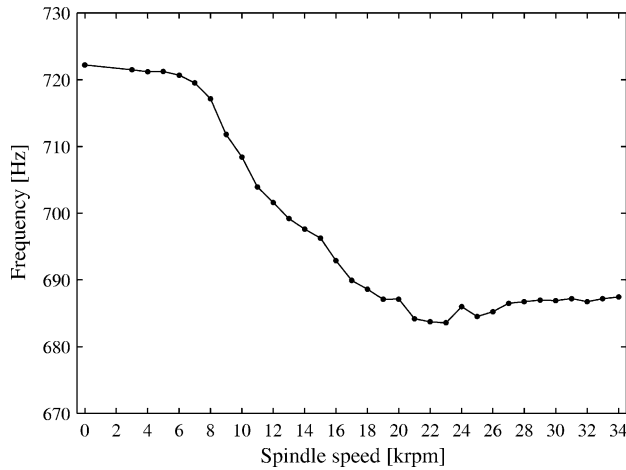


Fig. 8. Frequency of the dominant vibration mode of the rotating tool vs. spindle speed.

Decrease of the mode compliance with the increasing spindle speed (not shown) could also explain the systematic increase of the experimental stability minima with spindle speed, which was observed experimentally for all a_e .

3.4. Tool motion in X–Y plane

Three different types of tool motion corresponding to three cutting regimes were predicted by the SD method and observed experimentally: periodic chatter-free regime, quasi-periodic chatter and periodic chatter regimes. Typical examples of tool motion in X–Y plane for the three regimes are shown in Fig. 9, together with the stroboscopically sampled deflection in the feed (X) direction and the amplitude spectrum of X-deflection. Frequency of the stroboscope was set at the tooth passing frequency $f_{TP} = 1/T = Nn$, which is for a cutter with a single tooth ($N = 1$) equal to the spindle speed, $f_{TP} = n$. For the two periodic cases, the noise-free trajectories of the tool motion are shown superimposed on the recorded trajectories, providing a detailed picture of the path followed by the tool. The noise-free trajectories were obtained by a nonlinear filtering technique suitable for periodically forced processes [25]. All examples shown in Fig. 9 were taken from the up-milling cuts with $a_e = 0.05D$.

In chatter-free regime (top panels in Fig. 9), the tool oscillates periodically with the tooth passing frequency f_{TP} which means that the tool motion repeats itself after each tooth pass. This is confirmed by the stroboscopically sampled data points which are grouped in one compact cloud and their values remain approximately constant as cutting progresses (top panel B). The amplitude spectrum of the deflection contains peaks only at the multiples of f_{TP} (top panel C). In quasi-periodic chatter regime (middle panels), the tool moves on a torus defined by the tooth passing frequency f_{TP} and the dominant eigen-frequency f_t of the machine–tool system. The two frequencies usually have

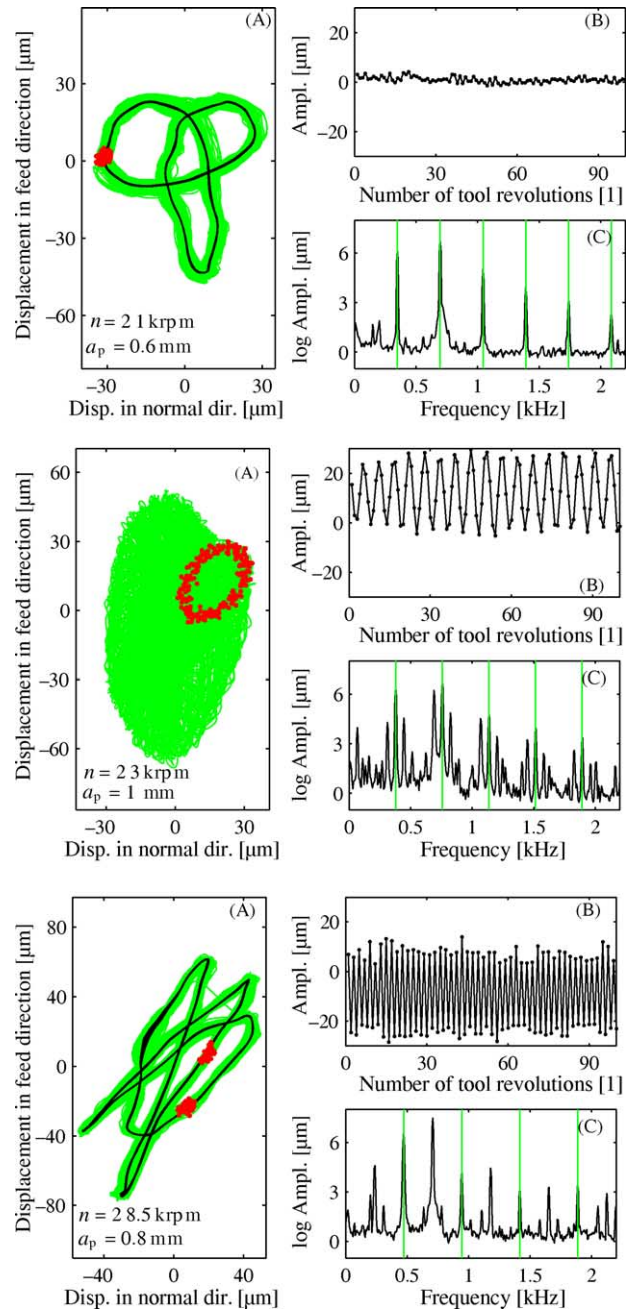


Fig. 9. Recorded tool motion (grey lines) in X–Y plane, with stroboscopically sampled data (dark dots) and the filtered tool motion (black lines) superimposed (A). Stroboscopically sampled X-deflection vs. time (B). Amplitude spectra of X-deflection; the grey vertical lines denote multiples of f_{TP} (C). Stable cutting (top), quasi-periodic chatter (middle), periodic chatter with period $2T$ (bottom); up-milling, $a_e = 0.05D$ (all).

incommensurate values. The stroboscopically sampled data points form an ellipse and their values oscillate in time (middle panel B). Peaks in the deflection spectrum are found at the two frequencies, f_{TP} and f_t , at their sums and differences, and multiples thereof (middle panel C). Tool motion in periodic chatter regime (bottom panels) is also periodic, but with twice the tooth passing period, $2T$ (or half the tooth passing frequency $f_{TP}/2$). This means that the tool

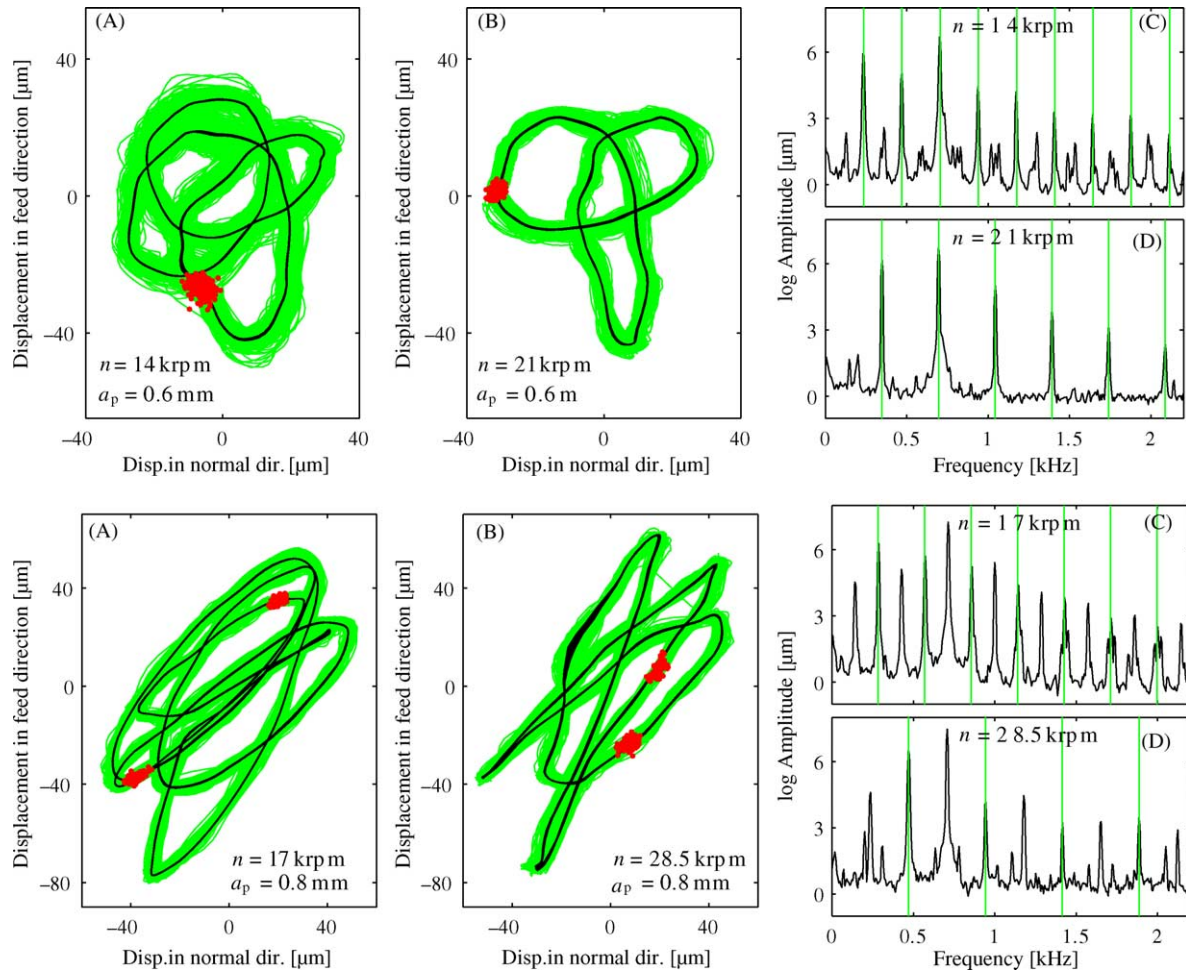


Fig. 10. Recorded tool motion (grey lines) in X–Y plane for two different lobes, with the stroboscopically sampled data (dark dots) and filtered tool motion (black lines) superimposed (A and B). The corresponding X-deflection amplitude spectra; the vertical lines denote multiples of f_{TP} (C and D). Stable cutting (top), periodic chatter (bottom); up-milling (all), $a_c = 0.05D$.

motion repeats itself after two tooth passes. The stroboscopically sampled data points form two compact clouds which are visited alternately by the tool trajectory (bottom panel B). The amplitude spectrum of the deflection shows peaks at the multiples of $f_{TP}/2$ (bottom panel C). Comparison of all three amplitude spectra (panels C) confirms that the tooth passing frequency is always present in the process, since it corresponds to the excited vibration of the tool, while the appearance of additional peaks in the spectra indicates chatter [26]. This well known property of milling dynamics is often exploited for the purpose of chatter detection.

In order to illustrate better the difference between the periodic chatter-free and periodic chatter regimes, tool motion at spindle speeds corresponding to two different lobes in the two regimes are compared in Fig. 10. The chatter-free examples (top panels) were taken from the stable regions at $n = f_t/3$ and $n = f_t/2$. In the $n = f_t/3$ case, the tool completes three oscillations per tooth pass period T

(top panel A), while two oscillations are completed in the $n = f_t/2$ case (top panel B). This is also reflected in the corresponding amplitude spectra of the tool deflection; the dominant eigen-frequency of the machine–tool system ($f_t \approx 722$ Hz) is matched respectively by the third (top panel C) and second harmonics (top panel D) of the tooth passing frequency f_{TP} . The periodic chatter examples (bottom panels) were taken from the flip bifurcation lobes predicted at $n = 2f_t/5$ and $n = 2f_t/3$, but observed at slightly lower spindle speeds. In the $n = 2f_t/5$ case, the tool completes two and a half oscillations per tooth pass period T , i.e. five oscillations per $2T$ (bottom panel A), while three oscillations are completed per $2T$ in the $n = 2f_t/3$ case (bottom panel B). The amplitude spectra show the highest peak at the eigen-frequency f_t matched respectively by the fifth (bottom panel C) and the third harmonics (bottom panel D) of half the tooth passing frequency $f_{TP}/2$.

Finally, three special cases of chatter observed experimentally are presented (Fig. 11): a combination of

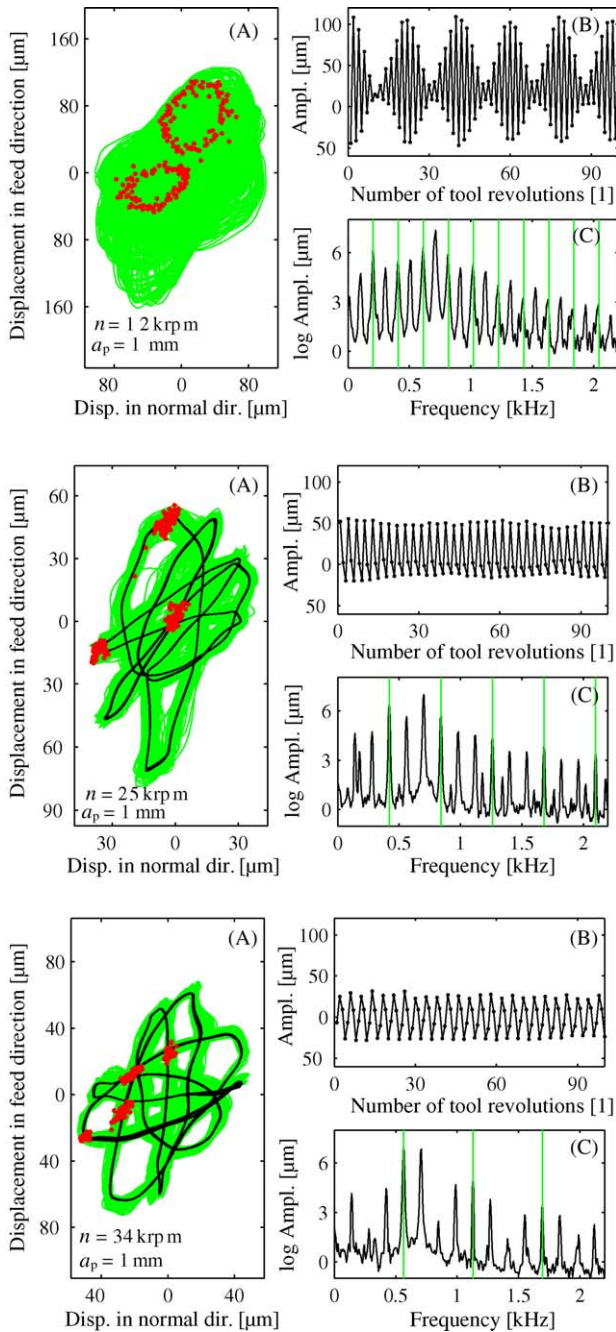


Fig. 11. Recorded tool motion in X–Y plane (grey lines), with stroboscopically sampled data (dark dots) and filtered tool motion (black lines) superimpose (A). Stroboscopically sampled X-deflection vs. time (B). Amplitude spectra of X-deflection; grey vertical lines denote multiples of f_{TP} (C). Combination of periodic and quasi-periodic chatter (top), periodic chatter with periodic $3T$ (middle), periodic chatter with period $4T$ (bottom); up-milling, $a_e = 0.05D$ (all).

the quasi-periodic and $2T$ periodic chatter, and two cases of periodic chatter with periods $3T$ and $4T$. Periodic chatter cases with higher periods were also observed but less frequently.

The combination of the quasi-periodic and periodic chatter types (top panels) was usually observed at cutting

depths above the flip bifurcation lobe. The stroboscopically sampled tool deflection indicates (top panel A) that during this type of chatter the tool moves on a torus defined by the dominant eigen-frequency f_i and half the tooth passing frequency $f_{TP}/2$. The peaks in the amplitude spectrum are located at the multiples of $f_{TP}/2$ (top panel C). Theoretically, such chatter could correspond to the case when at least one pair of complex conjugate eigen-values and at least one real eigen-value of the Floquet transition matrix (Eq. (20)) were in modulus larger than 1.

The periodic chatter cases with periods $> 2T$ are in fact special cases of the quasi-periodic chatter. They were observed mainly at low radial immersions and always within the Hopf bifurcation lobe, where the quasi-periodic type of chatter was expected. In Fig. 11, the examples with periods $3T$ (middle panels) and $4T$ (bottom panels) are shown. The stroboscopically sampled data points are gathered respectively in three and four compact clouds (panels A) visited periodically in time (panels B). The amplitude spectra of the X-deflection contain peaks at the multiples of $f_{TP}/3$ and $f_{TP}/4$, respectively (panels C). These properties are similar to those reported in Ref. [16] for the $3T$ periodic motion of a 1-dof milling system. The stability theory of milling does not predict periodic types of chatter with periods other than $2T$. The two cases shown here could correspond to the quasi-periodic chatter cases when the pair of complex conjugate eigen-values of the transition matrix penetrates the unit circle in the complex plane at angles $\pm 2\pi/3$ (period $3T$) and $\pm \pi/2$ (period $4T$, see bottom left panel of Fig. 3). In parlance of the dynamical systems theory [27], occurrence of these periodic chatter cases could be attributed to the fact that at low radial immersions the periodic motion synchronized with the periodic forcing attracts the trajectory more than the quasi-periodic motion which is unsynchronized with the forcing.

4. Conclusions

Stability of a 2-dof milling process was investigated. Stability boundaries were predicted by the zeroth order approximation (ZOA) and semi-discretization (SD) methods. While similar for high radial immersions, predictions of the two methods grow increasingly different as radial immersion is decreased. The most significant difference is an additional set of stability lobes predicted only by the SD method. These lobes correspond mainly to the type of instability called period doubling or flip bifurcation, which causes a periodic type of chatter, as opposed to the quasi-periodic chatter caused by the instability called Hopf bifurcation. More detailed numerical investigations also revealed that the flip bifurcation lobes are in fact closed curves distributed across the plane spanned by the spindle speed and axial depth of cut. It is not uncommon for the closed flip lobes to be located entirely within the stable parameter domain.

Experimental verification of the stability boundaries confirmed the predictions of the SD method. However, quantitative agreement between the predictions and experiments diminished as radial immersion was decreased. While structures of the predicted and experimental stability boundaries remained similar also at low radial immersions, the predicted stability maxima were much higher than those observed experimentally. The reasons for these quantitative discrepancies could possibly be attributed to the variation of the radial immersion during cutting due to the tool deflection and to the effects of edge (ploughing) forces that were not considered in the force model. The experiments also showed that the machine–tool modal properties may depend on spindle speed. In the present study, the frequency and compliance of the dominant vibration mode (first bending mode of the tool) were found to decrease as spindle speed was increased.

All three types of tool motion predicted by the SD method were observed experimentally: periodic chatter-free, quasi-periodic chatter and periodic chatter. Analysis of the tool deflections recorded during these motion types confirmed the properties predicted by the theory. In addition, three special cases of chatter were shown: a combination of quasi-periodic and periodic chatter types, observed above the flip bifurcation lobe, and two periodic chatter cases with higher periods, observed within the Hopf bifurcation lobe.

In summary, the presented investigations have shown that there indeed exist two types of instability in milling. In order to assure chatter-free machining, both of them should be taken into account when selecting the cutting parameters.

Acknowledgements

JG gratefully acknowledges the support of the Alexander von Humboldt Foundation. TI was supported by the Magyary Zoltán Postdoctoral Fellowship of the Foundation for Hungarian Higher Education and Research, and together with GS, also by the Hungarian National Science Foundation under grants no. OTKA F047318 and OTKA T043368. Authors would also like to thank Dr Etienne Balmès from SDTools, and Oliver Webber and Horst Helbing from ISF for their helpful comments.

References

- [1] J. Tlustý, M. Poláček, The stability of machine–tool against self-excited vibration in machining, in: Proceedings of the International Research in Production Engineering, American Society of Mechanical Engineers (ASME), Pittsburgh, USA, 1963, p. 465.
- [2] S.A. Tobias, Machine Tool Vibration, Blackie & Son, Ltd, London, 1965.
- [3] H.M. Shi, S.A. Tobias, Theory of finite amplitude machine tool instability, *International Journal of Machine Tools and Manufacture* 24 (1) (1984) 45–69.
- [4] G. Stépán, T. Kalmár-Nagy, Nonlinear regenerative machine tool vibrations, in: Proceedings of the 16th ASME Biennial Conference on Mechanical Vibration and Noise, 1997 ASME Design and Technical Conferences, Sacramento, CA, 1997, pp. 1–11.
- [5] J. Tlustý, F. Ismail, Basic non-linearity in machining chatter, *Annals of the CIRP* 30 (1) (1981) 299–304.
- [6] M.X. Zhao, B. Balachandran, Dynamics and stability of milling process, *International Journal of Solids and Structures* 38 (10–13) (2001) 2233–2248.
- [7] M.L. Campomanes, Y. Altıntaş, An improved time domain simulation for dynamic milling at small radial immersions, *ASME Journal of Manufacturing Science and Engineering* 125 (3) (2003) 416–422.
- [8] I.E. Minis, R. Yanushevsky, A new theoretical approach for the prediction of machine tool chatter in milling, *ASME Journal of Engineering for Industry* 115 (1) (1993) 1–8.
- [9] E. Budak, Y. Altıntaş, Analytical prediction of chatter stability in milling—part I: general formulation, *ASME Journal of Dynamic Systems, Measurements, and Control* 120 (1) (1998) 22–30.
- [10] E. Budak, Y. Altıntaş, Analytical prediction of chatter stability in milling—part II: application of the general formulation to common milling systems, *ASME Journal of Dynamic Systems, Measurements, and Control* 120 (1) (1998) 31–36.
- [11] Y. Altıntaş, E. Budak, Analytical prediction of stability lobes in milling, *Annals of the CIRP* 44 (1) (1995) 357–362.
- [12] M.A. Davies, J.R. Pratt, B. Dutterer, T.J. Burns, The stability of low radial immersion milling, *Annals of the CIRP* 49 (1) (2000) 37–40.
- [13] M.A. Davies, J.R. Pratt, B. Dutterer, T.J. Burns, Stability prediction for low radial immersion milling, *ASME Journal of Manufacturing Science and Engineering* 124 (2) (2002) 217–225.
- [14] P.V. Bayly, J.E. Halley, B.P. Mann, M.A. Davies, Stability of interrupted cutting by temporal finite element analysis, *ASME Journal of Manufacturing Science and Engineering* 125 (2) (2003) 220–225.
- [15] T. Insperger, G. Stépán, Semi-discretization method for delayed systems, *International Journal for Numerical Methods in Engineering* 55 (2002) 503–518.
- [16] T. Insperger, B.P. Mann, G. Stépán, P.V. Bayly, Stability of up-milling and down-milling, part 1; alternative analytical methods, *International Journal of Machine Tools and Manufacture* 43 (1) (2003) 25–34.
- [17] B.P. Mann, T. Insperger, P.V. Bayly, G. Stépán, Stability of up-milling and down-milling, part 2; experimental verification, *International Journal of Machine Tools and Manufacture* 43 (1) (2003) 35–40.
- [18] P.V. Bayly, B.P. Mann, T.L. Schmitz, D.A. Peters, G. Stépán, T. Insperger, Effects of radial immersion and cutting conditions on chatter instability of end-milling, in: ASME International Mechanical Engineering Conference and Exposition (IMECE02), New Orleans, USA, 2002.
- [19] B.P. Mann, P.V. Bayly, M.A. Davies, J.E. Halley, Limit cycles, bifurcations, and accuracy of the milling process, *Journal of Sound and Vibration* 277 (1) (2004) 31–48.
- [20] T. Insperger, G. Stépán, Updated semi-discretization method for periodic delay-differential equations with discrete delay, *International Journal of Numerical Methods in Engineering* 61 (1) (2004) 117–141.
- [21] O. Elbeyli, J.Q. Sun, On the semi-discretization method for feedback control design of linear systems with time delay, *Journal of Sound and Vibration* 273 (1–2) (2004) 429–440.
- [22] E. Budak, Y. Altıntaş, E.J.A. Armarego, Prediction of milling force coefficients from orthogonal cutting data, *ASME Journal of Manufacturing Science and Engineering* 118 (2) (1996) 216–224.

- [23] J. Gradišek, M. Kalveram, K. Weinert, Mechanistic identification of specific force coefficients for a general end mill, *International Journal of Machine Tools and Manufacture* 44 (4) (2004) 401–414.
- [24] R. Szalai, G. Stépán, Stability boundaries of high-speed milling corresponding to period doubling are essentially closed curves, in: *Proceedings of IMECE2003, ASME International Mechanical Engineering Congress*, Washington, DC, USA, 2003.
- [25] J. Gradišek, R. Friedrich, E. Govekar, I. Grabec, Analysis of data from periodically forced stochastic processes, *Physics Letters A* 294 (3–4) (2002) 234–238.
- [26] T. Insperger, G. Stépán, P.V. Bayly, B.P. Mann, Multiple chatter frequencies in milling process, *Journal of Sound and Vibration* 262 (2) (2003) 333–345.
- [27] E. Ott, *Chaos in Dynamical Systems*, Cambridge University Press, Cambridge, 1993.